

# Fu–Kane–Mele monopoles in semimetals

Guo Chuan Thiang,<sup>1</sup> Koji Sato,<sup>2</sup> and Kiyonori Gomi<sup>3</sup>

<sup>1</sup>*School of Mathematical Sciences, University of Adelaide, SA 5000, Australia*

<sup>2</sup>*Institute for Materials Research, Tohoku University, Sendai 980-8577, Japan*

<sup>3</sup>*Department of Mathematical Sciences, Shinshu University, Matsumoto, Nagano 390-8621, Japan*

In semimetals with time-reversal symmetry, the interplay between Weyl points and Fu–Kane–Mele indices results in coexisting surface Dirac cones and Fermi arcs that are transmutable without a topological phase transition. The Weyl points’ connectivity is essential for capturing the full topology of semimetals and their role as intermediaries of topological insulator transitions. We also predict the possibility of a topological Dirac cone on the interface between two Weyl semimetals.

The groundbreaking discoveries of topological phases of matter in the last decade have fuelled intense research activity in theoretical and experimental condensed matter physics. Topological insulators and superconductors, whose spectra have energy gaps, have unusual properties arising from topological invariants depending on both symmetries and dimension [1, 2]. More recently, topological *semimetals* have received a lot of attention due to them hosting exotic fermions as quasiparticles. For *Weyl* semimetals (WSM) with broken  $\mathbf{T}$  (time-reversal) symmetry, proposals include pyrochlore iridates [3, 4] and multilayer structures of topological insulators with ferromagnetic order and normal insulators [5, 6];  $\mathbf{T}$ -symmetric WSM (T-WSM) were proposed in Ref. 7.

3D WSMs have topologically protected band crossings [3, 8]: a two-band Bloch Hamiltonian  $H(k) = \mathbf{h}(k) \cdot \boldsymbol{\sigma}$ ,  $k \in \mathbb{T}^3$  is specified by a 3-component vector field  $\mathbf{h}$  over the Brillouin zone (BZ)  $\mathbb{T}^3$ , with  $\boldsymbol{\sigma}$  the vector of Pauli matrices. Since the spectrum is  $\pm|\mathbf{h}(k)|$ , band crossings occur at a set  $W \subset \mathbb{T}^3$  of *Weyl points* where  $\mathbf{h} = \mathbf{0}$ . The *Weyl charge* of  $w \in W$  is the degree (2D winding number) of  $\hat{\mathbf{h}} = \mathbf{h}/|\mathbf{h}|$  restricted to a small 2-sphere  $S_w^2$  around  $w$ , and equals the Chern number of the valence band restricted to  $S_w^2$ , so  $w$  is a monopole for the band’s Berry curvature  $\mathcal{F}$ . A charge-cancellation condition [9] means that a *topological* WSM has at least two oppositely-charged Weyl points. It was predicted that *Fermi arcs* of surface states would connect the projected Weyl points on the surface BZ [3, 5].

The experimental discovery of Fermi arcs in T-WSM [10–12] leads naturally to a search for materials with *both* Fermi arcs and Dirac cones; the latter are associated with  $\mathbf{T}$ -symmetric topological insulators (TI). Such systems have been studied on the interface of a WSM-TI heterostructure [13] and in T-WSM [14, 15]. However, the topological index there and in general T-WSMs is not understood precisely. We solve this problem in this Letter, by defining topological invariants carefully for T-WSM, and computing them to be  $\mathbb{Z}_2^4 \oplus \mathbb{Z}$  for the simplest T-WSM. Our analysis reveals how Weyl points and Fu–Kane–Mele invariants (FKMI) interact in a subtle way with dramatic consequences for the surface states. Dirac cones and Fermi arcs are not “topo-

logically independent”, but can transmute between each other without the bulk invariants changing, c.f. the “dangling Dirac cone” found in [14]. We also provide a new *arc-representation* of T-WSM, which directly links to TI phase transitions and the surface Fermi arc-Dirac cone topology. Finally, we predict and provide numerical evidence that Fermi arcs can combine into a solitary surface Dirac cone on the interface between two T-WSM.

Hamiltonians with  $\mathbf{T}$ -symmetry ( $\mathbf{T}^2 = -1$ ) obey  $\mathbf{T}H(k)\mathbf{T}^{-1} = H(\tau(k))$  with  $\tau(k) = -k$ . In  $d$ -dimensions, there are  $2^d$  **T**ime **R**eversal **I**nvariant **M**omenta (TRIM) with  $k = -k$ . The basic 2D/3D TI has two valence bands by Kramers degeneracy. Although Bloch eigenstates  $|u_a(k)\rangle$ ,  $a = 1, 2$  are smoothly definable on the whole BZ (Chern numbers vanish), the “ $\mathbf{T}$ -gauge condition”  $|u_1(-k)\rangle = \mathbf{T}|u_2(k)\rangle$  may fail. From the matrix function  $\omega(k) \equiv (\omega_{ab}(k)) = \langle u_a(-k)|\mathbf{T}|u_b(k)\rangle$ , each TRIM gets a  $\pm$  sign given by  $\sqrt{\det(\omega)}/\text{Pf}(\omega)$  there. These signs depend on the choice of  $|u_a(k)\rangle$ , but in 2D the product-of-signs (POS), called the 2D FKMI  $\nu$ , is *gauge invariant* [16–18]; it also equals an **E**ffective **B**Z (EBZ) (e.g. front face of Fig. 4(a)) integral,

$$\nu = (-1)^\Delta, \quad \Delta = \frac{1}{2\pi} \left( \oint_{\partial\text{EBZ}} \mathcal{A} - \int_{\text{EBZ}} \mathcal{F} \right) \text{ mod } 2. \quad (1)$$

The loop integral of the Berry connection  $\mathcal{A}$  is computed in a  $\mathbf{T}$ -gauge over the EBZ boundary (comprising two loops), and is gauge-invariant mod 2 ([16] Appendix).

A  $\mathbf{T}$ -stable subspace  $Y$  has  $\tau(y) \in Y$  whenever  $y \in Y$ ; e.g. the  $k_i = 0$  or  $\pi$ ,  $i \in \{x, y, z\}$  planes (actually 2D tori) in the 3D BZ, which we call  $\mathbf{T}$ -planes. Applying  $\nu$  to them gives six  $\mathbb{Z}_2$ -numbers  $\nu_{i,0}, \nu_{i,\pi}$ . They obey  $\nu_{i,0} = \nu_0 \nu_{i,\pi}$ , where  $\nu_0$  is the *strong* FKMI defined as the POS of all eight TRIM in the 3D BZ [17]. Thus 3D TI are labelled by  $(\nu_0; \nu_i) \in \mathbb{Z}_2^4$ , with  $\nu_i \equiv \nu_{i,\pi}$  the three *weak* FKMI.

For a valence band *without*  $\mathbf{T}$ -symmetry,  $\frac{\mathcal{F}}{2\pi}$  integrates to an integer (a *Chern number*) over *any* closed surface in the BZ. In 3D, there are three independent (weak) Chern numbers  $c_1^{xy}, c_1^{yz}, c_1^{zx}$  corresponding to the 2D subtorus at (any) fixed  $k_z, k_x, k_y$  respectively. Valence bands of WSM are only defined over  $\mathbb{T}^3 \setminus W$ , and there is an extra Chern number on each  $S_w^2$  (the Weyl charge of  $w$ ). Then  $c_1^{xy}$  depends on  $k_z$ , jumping by the Weyl charge when

the constant  $k_z$  subtorus is moved past  $w$ ; similarly for  $c_1^{yz}, c_1^{zx}$ . If a closed surface encloses zero net Weyl charge, the valence bands can be extended into the whole interior by annihilating oppositely-charged pairs of enclosed Weyl points and opening a gap. In reverse, Weyl point pairs can be created by gap closing and then separated, their “history” being a set of connections between  $\pm$  Weyl pairs, oriented according to net positive charge motion (so they point from  $-$  to  $+$ ). Even a single Weyl pair has several topologically distinct connections due to the periodic BZ directions, leading to topologically distinct WSM [19, 20].

The simplest T-WSM has four Weyl points  $\pm w, \pm w'$ , away from TRIM and T-planes at  $k_i = 0, \pi$  (Fig. 1(a));  $\pm w$  (resp.  $\pm w'$ ) each has charge  $q \in \mathbb{Z}$  (resp.  $-q$ ) [7, 14, 21]. It has 2D FKMI  $\nu_{i,0}, \nu_{i,\pi}$  by restricting to respective T-planes. However, the strong FKMI  $\nu_0$  cannot be defined this way, because the Weyl charges prevent  $|u_1(k)\rangle, |u_2(k)\rangle$  from existing globally on  $\mathbb{T}^3 \setminus W$ . To proceed, we first locally “cordon off” the Weyl points in charge-cancelling pairs by some disjoint T-stable surfaces (T-surfaces)  $S$  that avoid the TRIM, e.g. the “vertical” brown surfaces in Fig. 2 (center). Then  $|u_a(k)\rangle$  can be globally defined *on* and *outside* of  $S$  since all the Chern numbers vanish, so we can calculate signs for all eight TRIM. We then *define*  $\nu_0$  for the T-WSM to be the POS — this coincides with the strong FKMI  $\nu_0^{\text{TI}}$  for the resulting TI after the Weyl points annihilate within  $S$ . There is, however, a crucial ambiguity in pairing up the Weyl points, whose consequence is best illustrated by the trivial  $\rightarrow$  strong TI transition described in [7], c.f. [22]. Starting from the intermediate T-WSM (Fig. 2, center), two ways (horizontal/vertical) of annihilating the Weyl points result in TIs which differ by a strong FKMI! We proceed with the “vertical” pairing convention, and resolve this  $\nu_0$  ambiguity afterwards.

In Refs. 13 and 14, it was found that the TI relation  $\nu_{i,0}^{\text{TI}} = \nu_0^{\text{TI}} \nu_{i,\pi}^{\text{TI}}$  no longer holds for T-WSM, suggesting that all six numbers  $\nu_{i,0}, \nu_{i,\pi}$  may become “independent”. In fact, only *three* are independent for a given  $W$ , the precise relation for the Fig. 1(a) example being

$$\nu_{x,0} = \nu_0 \nu_{x,\pi}; \quad \nu_{i,0} = (-1)^q \nu_0 \nu_{i,\pi}, \quad i = y, z, \quad (2)$$

The extra  $(-1)^q$  factors in Eq. (2) may be understood by thinking of Weyl points as “monopoles” for the 2D FKMI invariant. Observe that there is a *continuum* of *curved* T-planes besides the standard flat ones (Fig. 1). Each curved T-plane with no Weyl points also has its own 2D FKMI, stable under T-plane deformation. For each  $i = x, y, z$ , consider a blue and a purple T-plane whose EBZs share the *same* boundary and jointly enclose  $w$  (Fig. 1). From Eq. (1), their respective  $\Delta$  satisfy

$$\Delta_{\text{purple}}^{i,0} - \Delta_{\text{blue}}^{i,0} = \int_{\substack{\text{purple EBZ} \\ \text{- blue EBZ}}} \mathcal{F} = \int_{\text{joint EBZ}} \mathcal{F} = q \pmod{2},$$

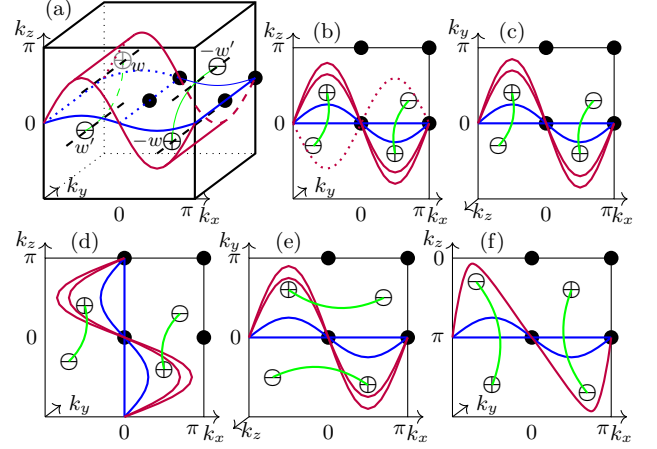


FIG. 1. (a) Purple/blue T-planes have the same EBZ boundaries. Their joint EBZ (left half planes) enclose  $w$  and has Chern number  $q$ . The 2D FKMI jumps by  $(-1)^q$  as a blue T-plane is deformed across  $\pm w$  into a purple one. (b)-(d) 2D BZ sections; green paths indicate how Weyl points are to be annihilated “vertically”. (e) Horizontal annihilation leads to a different TI. (f) A “vertical” path passing through  $k_z = \pi$ .

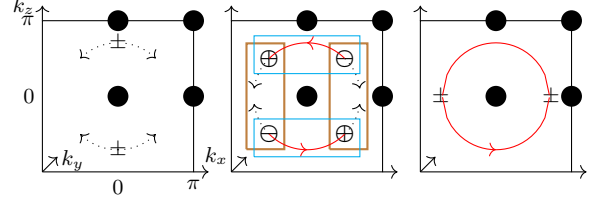


FIG. 2. [L-R] Two  $\pm$  pairs of Weyl points are created from a trivial TI, moved apart along the dotted arrows to form a T-WSM, then annihilated to form a strong TI. Their history traces out a circle (red) which represents the acquisition of a strong FKMI. The brown and cyan T-surfaces are two inequivalent ways to enclose cancelling pairs of Weyl points.

where the loop integral contributions cancel and the joint EBZ is oriented with outward normal [23]. It follows that

$$\nu_{i,0} = \nu_{i,0}^{\text{blue}} = (-1)^{\Delta_{\text{blue}}^{i,0}} = (-1)^{\Delta_{\text{purple}}^{i,0} - q} = (-1)^q \nu_{i,0}^{\text{purple}} \quad (3)$$

Use a “vertical” Weyl point annihilation path that passes through the T-planes  $k_z = 0, k_y = 0$  but not  $k_x = 0$  (Fig. 1(a)-(d)), to obtain a TI with FKMI  $\nu_0^{\text{TI}}, \nu_{i,0}^{\text{TI}}, \nu_{i,\pi}^{\text{TI}}$ . Then  $\nu_0 = \nu_0^{\text{TI}}$  and  $\nu_{i,\pi} = \nu_{i,\pi}^{\text{TI}}$ , but  $\nu_{i,0}$  requires care. From Fig. 1(b)-(c), only the purple T-planes persist in the TI and deform to flat ones, whereas the blue ones survive in Fig. 1(d). Thus  $\nu_{y/z,0}^{\text{purple}} = \nu_{y/z,0}^{\text{TI}} = \nu_0^{\text{TI}} \nu_{y/z,\pi}^{\text{TI}} = \nu_0 \nu_{y/z,\pi}$  but  $\nu_{x,0}^{\text{blue}} = \nu_{x,0}^{\text{TI}} = \nu_0^{\text{TI}} \nu_{x,\pi}^{\text{TI}} = \nu_0 \nu_{x,\pi}$ , which together with Eq. (3) gives Eq. (2). We conclude that T-WSM are completely labelled by  $(\nu_0; \nu_i; q) \in \mathbb{Z}_2^4 \oplus \mathbb{Z}$  where  $\nu_i \equiv \nu_{i,\pi}$ . A different configuration  $W'$  generally leads to some other splitting of cases in Eq. (2). Also, if some of the flat T-planes contain Weyl points, we can replace the ill-defined  $\nu_{i,0}, \nu_{i,\pi}$  by the 2D FKMI of slightly curved T-planes which avoid  $W$ .

Formally, a valence band over  $X$  without T-symmetry

is classified by the *second cohomology group*  $H^2(X)$ . The analogous group for T-invariant valence bands [18, 24], denoted  $\mathcal{H}^2(X)$ , may be computed (see [25]) to be  $\mathcal{H}^2(\mathbb{T}^2) \cong \mathbb{Z}_2$ ,  $\mathcal{H}^2(\mathbb{T}^3) \cong \mathbb{Z}_2^4$  for TI, and  $\mathcal{H}^2(\mathbb{T}^3 \setminus W) \cong \mathbb{Z}_2^4 \oplus \mathbb{Z}$  for T-WSM, consistent with the above arguments. Abstractly, the dual *homology groups*  $\mathcal{H}_1$  do the same job [25], and we demonstrate this from a physical viewpoint which does not require detailed knowledge of  $\mathcal{H}^2, \mathcal{H}_1$ .

Define  $\nu'_0$  for the T-WSM to be the strong FKMI of the TI that results from annihilating Weyl points *horizontally* (Fig. 1(e)). We expect (from Fig. 2) that  $\nu'_0 = (-1)^q \nu_0$ . Indeed, repeating the above procedures yields  $\nu_{x,0} = (-1)^q \nu'_0 \nu_{x,\pi}$  and  $\nu_{y/z,0} = \nu'_0 \nu_{y/z,\pi}$ , which is exactly Eq. (2) with  $\nu'_0 = (-1)^q \nu_0$ . Next, consider a vertical annihilation path passing through  $k_z = \pi$  instead of  $k_z = 0$  (Fig. 1(f)). Then it is instead the curved (flat) T-plane that corresponds to  $\nu_{z,\pi}^{\text{TI}}$  ( $\nu_{z,0}^{\text{TI}}$ ), so to end up at the same TI that the original vertical path produced, we need to start from a *different* T-WSM with  $\nu_{z,0/\pi}$  replaced by  $(-1)^q \nu_{z,0/\pi}$ ; similarly for paths through  $k_{x/y} = \pi$ . Thus the Weyl point annihilation (creation) path affects the resultant TI (T-WSM), as suggested in [7, 22], so TI/T-WSM can also be classified via Weyl point paths up to T-invariant deformations.

Closed arcs/paths (i.e. loops)  $l$  in a space  $X$  are classified up to deformation by the first *homology group*  $H_1(X)$  [26]; e.g. there are three independent non-contractible loops in  $\mathbb{T}^3$ , so  $H_1(\mathbb{T}^3) \cong \mathbb{Z}^3$ . For WSM, arcs connecting Weyl points are allowed (“ $W$ -relative loops” [27]), so the *relative group*  $H_1(\mathbb{T}^3, W)$  is required. For TI/T-WSM, *equivariant homology groups* [25], denoted  $\mathcal{H}_1(\mathbb{T}^3), \mathcal{H}_1(\mathbb{T}^3, W)$ , classify T-stable loops. Equivalently, we can classify loops  $\check{l}$  in the *quotient space*  $\check{\mathbb{T}}^3$  of the BZ under  $\tau$ , i.e. the 3D EBZ with  $k \sim \tau(k)$  identifications at the boundary faces (Fig. 4(a)), since  $\check{l}$  in  $\check{\mathbb{T}}^3$  “doubles” into a T-stable loop  $l = \check{l} \cup \tau(\check{l})$  in  $\mathbb{T}^3$ . Each pair  $(k, \tau(k))$  in the BZ is “halved” into a single point in  $\check{\mathbb{T}}^3$ , with the caveat that “halving a TRIM” properly requires the *homotopy quotient* rather than  $\check{\mathbb{T}}^3$ . For our purposes, it suffices to look at loops in  $\check{\mathbb{T}}^3$  (or T-stable loops in  $\mathbb{T}^3$ ) which *avoid* the TRIM. We will see that  $\mathcal{H}_1(\mathbb{T}^3) \cong \mathbb{Z}_2^4$  and  $\mathcal{H}_1(\mathbb{T}^3, W) \cong \mathbb{Z}_2^4 \oplus \mathbb{Z}$ , exactly mirroring the classification of TI and T-WSM (by  $\mathcal{H}^2$ ). This apparent coincidence is due to a deep result called *Poincaré duality* (PD) [25, 28, 29], see [30] for PD applied to electromagnetic theory. In the T-broken case, PD identifies  $H^2(\mathbb{T}^3) \cong H_1(\mathbb{T}^3) \cong \mathbb{Z}^3$ . For the T-symmetric case, PD identifies  $\mathcal{H}^2(\mathbb{T}^3)$  and  $\mathcal{H}^2(\mathbb{T}^3 \setminus W)$  with  $\mathcal{H}_1(\mathbb{T}^3)$  and  $\mathcal{H}_1(\mathbb{T}^3, W)$  [31].

For each  $i = x, y, z$ , let  $l_i$  be a T-stable pair of loops winding around  $k_i$ , and consider its deformations through T-stable loops. It cannot be contracted to a point without hitting TRIMs, but does rotate onto its oppositely-oriented self  $l_i^{\text{op}}$  (Fig. 3(a)). Thus *two* copies of  $l_i$  deform into  $l_i + l_i^{\text{op}}$ , which *together* is T-stably contractible, so  $l_i$

generates  $\mathbb{Z}_2 \subset \mathcal{H}_1(\mathbb{T}^3)$ ; this  $\mathbb{Z}_2$  is dual to the weak FKMI  $\nu_i$ . Next, a T-stable equator  $l_0$  of a 2-sphere surrounding the TRIM at  $\mathbf{0}$  cannot be contracted T-stably without hitting the TRIM. All equators are equivalent since one can be rotated onto another (Fig. 3(b)); in particular,  $l_0$  is equivalent  $l_0^{\text{op}}$ , so  $l_0$  also generates a  $\mathbb{Z}_2 \subset \mathcal{H}_1(\mathbb{T}^3)$ , dual to the strong FKMI  $\nu_0$ . Projected onto the surface BZ,  $l_0$  gives the Fermi surface of a surface Dirac cone pinned to  $(0, 0)$  while  $l_i$  gives that of weak TI exactly as in [1, 17]. An equator encircling any other TRIM is not another independent loop, but is deformable to some combination of  $l_0$  and  $l_i$  (Fig. 3(c)), thus  $\mathcal{H}_1(\mathbb{T}^3) \cong \mathbb{Z}_2^4$ . For T-WSM with  $W = \{\pm w, \pm w'\}$ , a T-stable pair of vertical arcs joining  $\pm w'$  to  $\pm w$  generates  $\mathbb{Z}$  in  $\mathcal{H}_1(\mathbb{T}^3, W) \cong \mathbb{Z}_2^4 \oplus \mathbb{Z}$ , dual to  $q$ , while the horizontal arc-pair joining  $\pm w'$  to  $\mp w$  is a combination of the vertical one and  $l_0$  (Fig. 3(e)); the Weyl point connections prefigure the surface Fermi arcs.

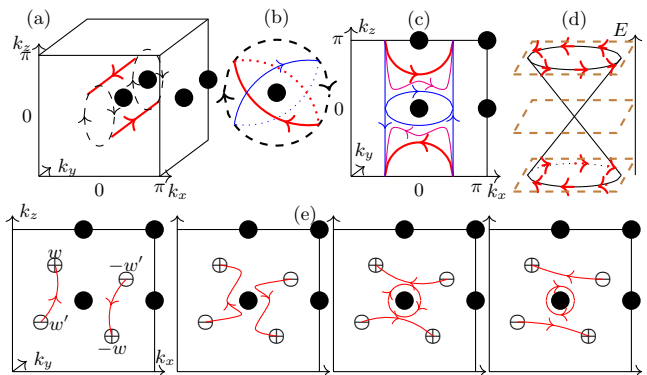


FIG. 3. (a) A T-stable pair of loops (red, dual to  $\nu_y$ ) rotates about the  $k_y$ -axis onto its oppositely-oriented self. (b) Red equator encircling TRIM at  $\mathbf{0}$ , dual to  $\nu_0$ , rotates onto any other equator (blue). (c) Red equator surrounding  $(0, 0, \pi)$  TRIM deforms into sum of blue equator around  $\mathbf{0}$  and blue loops along  $k_z$ . (d) Helical Dirac cone with spin texture (red). (e) Vertical Weyl point connection deforms into horizontal connection plus a circle dual to  $\nu_0$ , numerically reproduced in Fig. 5(e).

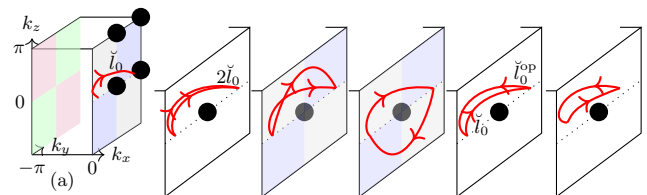


FIG. 4. (a) The quotient  $\check{\mathbb{T}}^3$  of the BZ under  $\tau$  is the 3D EBZ with further identifications  $(k_y, k_z) \sim (-k_y, -k_z)$  at each EBZ boundary face  $k_x = 0, -\pi$ . Since its end points are identified, the red arc is a closed loop  $\check{l}_0$  in  $\check{\mathbb{T}}^3$ , which is “half” of the equator  $l_0$  surrounding  $\mathbf{0}$ . Starting from *two* such loops, deform one  $\check{l}_0$  into a loop on the  $k_x = 0$  face, identify it with its inverted self, then deform it back to  $\check{l}_0^{\text{op}}$ . Thus  $2\check{l}_0 \sim \check{l}_0 + \check{l}_0^{\text{op}}$ , which is contractible in  $\check{\mathbb{T}}^3$ .

We can also see why  $l_0, l_i$  each generates  $\mathbb{Z}_2$ , by considering their respective “halves”  $\check{l}_0, \check{l}_i$  in  $\check{\mathbb{T}}^3$ . For example, Fig. 4 shows how a loop going around  $\check{l}_0$  *twice* is con-

tractable, see [25] for the  $\check{l}_i$  case. This is just like  $\text{SO}(3)$ , the quotient of  $\text{SU}(2)$  by  $\mathbb{Z}_2$ , having a loop which only becomes contractible after looping twice.

In this arc-representation of TI/T-WSM, the FKMI on any T-plane is simply the number of intersection-pairs (mod 2) between the arcs and the T-plane, e.g. the red loops in Fig. 3(a) represent a weak TI with  $(\nu_0; \nu_i) = (+; +, -, +)$ , while the equator around  $(0, 0, \pi)$  represents a strong TI with  $(\nu_0; \nu_i) = (-; +, +, -)$  (Fig. 3(c)). Intersection numbers are another formulation of PD, were used implicitly in characterising the surface Fermi surface of a TI by intersection properties with certain lines in the surface BZ [1, 16, 17], and applied explicitly in semimetals in [20].

In the T-broken case, the bulk-boundary correspondence involves integrating (e.g. 2D Berry curvature) transversally (say  $k_y$ ), to obtain a boundary invariant (e.g. 1D winding number), c.f. dimensional reduction [32], charge pumping [33], Zak phase computation [34], spectral flow/Toeplitz index [25, 35–38]. With T-symmetry, we need to “integrate out  $k_y$  T-invariantly”, c.f. the spin pump [16] generalising [33]). Integration of a differential form along  $k_y$  transforms under PD into the map  $p$  projecting out  $k_y$  [25, 28]. This indicates why the surface Fermi surface can be found by dualising a T-WSM into arcs and then projecting onto the surface BZ,

$$\mathcal{P} : \underbrace{\mathcal{H}^2(\mathbb{T}^3 \setminus W)}_{\text{Bulk invariants}} \xrightarrow[\text{PD}]{} \underbrace{\mathcal{H}_1(\mathbb{T}^3, W)}_{\text{arc representation}} \xrightarrow{p} \underbrace{\mathcal{H}_1(\mathbb{T}^2, p(W))}_{\text{boundary invariants}}$$

The T-WSM generically has four projected Weyl points, then  $\mathcal{H}_1(\mathbb{T}^2, p(W)) \cong \mathbb{Z}_2 \oplus \mathbb{Z}_2^2 \oplus \mathbb{Z}$ : the first factor is  $\mathcal{P}(\nu_0)$  (loop around  $(k_x, k_z) = (0, 0)$ ), the middle factor is  $\mathcal{P}(\nu_x), \mathcal{P}(\nu_z)$  (loop-pairs wrapping  $k_x, k_z$ ), the last factor is  $\mathcal{P}(q)$  (Fermi arc-pair from  $p(\pm w')$  to  $p(\pm w)$ ), while  $\nu_y$  does not contribute since it corresponds to a weak TI built from layers of 2D TI parallel to the boundary.

Recall that the *helical* Dirac cone of a strong TI has spin-momentum locking in opposite senses for the two halves of the cone [1, 39] (Fig. 3(d)). As the Fermi energy is varied slightly, the Fermi surface (a loop oriented along the spin) undergoes a “Lifshitz transition” first to a Dirac point, then to an oppositely-oriented loop. All these surfaces arise from the same bulk Hamiltonian, and their interpolation as mediated by the Dirac cone realises their topological equivalence. The Dirac point (as a degenerate loop) is *essential* for the Fermi loop orientation to change continuously so that such a loop has a  $\mathbb{Z}_2$  index.

Under a continuous change of the bulk Hamiltonian, neither the T-WSM indices nor the dual arcs’ topology changes. It is then easy, for more complicated Weyl point configurations, to recognise which Fermi arc-Dirac cone configurations are continuous “rewirings” of one another (by deforming the T-WSM Hamiltonian) [40], and which ones require a genuine topological phase transitions [20].

Consider two distinct T-WSM A and B, with respective indices  $(+; +, +, +; 1)$  and  $(-; +, +, +; 1)$ . At their

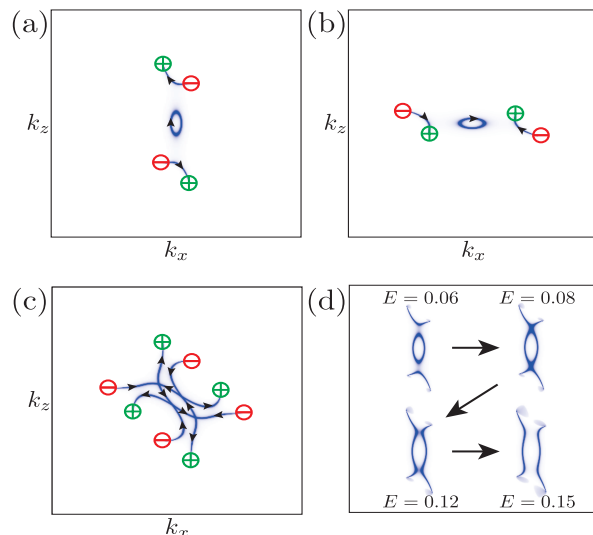


FIG. 5. (a) Surface Fermi surface of T-WSM A corresponding to the right most figure in Fig. 3(e) with two Fermi arcs and a single Dirac cone. (b) Fermi surface on opposite surface of T-WSM B, obtained from A by reflecting. (c) Interface Fermi surface of the system obtained by stacking A and B. (d) Fermi surfaces of A at various Fermi energies, reproducing the deformation sequence of Fig. 3(e).

interface (transverse to  $y$ ), we expect the Fermi surface to be the *difference*  $\mathcal{P}(+; +, +, +; 1) - \mathcal{P}(-; +, +, +; 1) = (-; +, +, +; 0)$ , i.e., a single Dirac cone. Using Hamiltonians from [14] to realise A (resp. B) with Fermi surfaces comprising a Dirac cone and horizontally (resp. vertically) connected Fermi arcs respectively, as in Fig. 5(a)-(b), we numerically analyse, using Green’s function methods [41], the interface-localised Fermi surface of the system with A stacked on top of B in the  $y$ -direction, obtaining Fig. 5(c). Instead of the Dirac cone from A annihilating that from B, we see that there is still a loop around  $(k_x, k_z) = (0, 0)$  corresponding to a single Dirac cone, while the remaining “rewired” Fermi arcs can be thought of as being contractible if the projected Weyl points of A had lined up exactly with those of B.

We have explained how Weyl points act as monopoles for 2D FKMI, leading to a  $\mathbb{Z}_2^4 \oplus \mathbb{Z}$  classification of T-WSM with four Weyl points. The Weyl points’ history provides a dual classification in terms of arcs, which prefigure the surface Fermi surface. By “rewiring” Fermi arcs, Dirac cones can be produced/destroyed without a topological phase transition. Finally, we have numerically confirmed our theoretical prediction that Fermi arcs at a T-WSM interface can combine to produce an extra Dirac cone.

G.C.T. was supported by ARC grant DE170100149, K.S. by Grants-In-Aid for Scientific Research (Grant No. 15K13531) from the MEXT, Japan, and K.G. by JSPS KAKENHI Grant No. JP15K04871. G.C.T. also thanks AIMR, Tohoku University for its hospitality.

- 
- [1] M. Z. Hasan and C. L. Kane, *Rev. Mod. Phys.* **82**, 3045 (2010).
- [2] X.-L. Qi and S.-C. Zhang, *Rev. Mod. Phys.* **83**, 1057 (2011).
- [3] X. Wan, A. M. Turner, A. Vishwanath, and S. Y. Savrasov, *Phys. Rev. B* **83**, 205101 (2011).
- [4] K.-Y. Yang, Y.-M. Lu, and Y. Ran, *Phys. Rev. B* **84**, 075129 (2011).
- [5] A. A. Burkov and L. Balents, *Phys. Rev. Lett.* **107**, 127205 (2011).
- [6] G. Xu, H. Weng, Z. Wang, X. Dai, and Z. Fang, *Phys. Rev. Lett.* **107**, 186806 (2011).
- [7] G. B. Halász and L. Balents, *Phys. Rev. B* **85**, 035103 (2012).
- [8] O. Vafek and A. Vishwanath, *Annu. Rev. Condens. Matter Phys.* **5**, 83 (2014).
- [9] H. Nielsen and M. Ninomiya, *Nucl. Phys. B* **193**, 173 (1981).
- [10] B. Q. Lv, H. M. Weng, B. B. Fu, X. P. Wang, H. Miao, J. Ma, P. Richard, X. C. Huang, L. X. Zhao, G. F. Chen, Z. Fang, X. Dai, T. Qian, and H. Ding, *Phys. Rev. X* **5**, 031013 (2015).
- [11] S.-Y. Xu, I. Belopolski, N. Alidoust, M. Neupane, G. Bian, C. Zhang, R. Sankar, G. Chang, Z. Yuan, C.-C. Lee, S.-M. Huang, H. Zheng, J. Ma, D. S. Sanchez, B. Wang, A. Bansil, F. Chou, P. P. Shibayev, H. Lin, S. Jia, and M. Z. Hasan, *Science* **349**, 613 (2015).
- [12] C.-L. Zhang, S.-Y. Xu, I. Belopolski, Z. Yuan, Z. Lin, B. Tong, G. Bian, N. Alidoust, C.-C. Lee, S.-M. Huang, T.-R. Chang, G. Chang, C.-H. Hsu, H.-T. Jeng, M. Neupane, D. S. Sanchez, H. Zheng, J. Wang, H. Lin, C. Zhang, H.-Z. Lu, S.-Q. Shen, T. Neupert, M. Zahid Hasan, and S. Jia, *Nat. Commun.* **7**, 10735 (2016).
- [13] A. G. Grushin, J. W. F. Venderbos, and J. H. Bardarson, *Phys. Rev. B* **91**, 121109 (2015).
- [14] A. Lau, J. van den Brink, and C. Ortix, *arXiv:1701.01660*.
- [15] X.-L. Sheng, Z.-M. Yu, R. Yu, H. Weng, and S. A. Yang, *ArXiv e-prints* (2017), *arXiv:1703.09040*.
- [16] L. Fu and C. L. Kane, *Phys. Rev. B* **74**, 195312 (2006).
- [17] L. Fu, C. L. Kane, and E. J. Mele, *Phys. Rev. Lett.* **98**, 106803 (2007).
- [18] G. De Nittis and K. Gomi, *Commun. Math. Phys.* **339**, 1 (2015).
- [19] V. Mathai and G. C. Thiang, *J. Phys. A: Math. Theor. (Letter)* **50**, 11LT01 (2017).
- [20] V. Mathai and G. C. Thiang, *arXiv:1611.08961*.
- [21] S. Kourtis, J. Li, Z. Wang, A. Yazdani, and B. A. Bernevig, *Phys. Rev. B* **93**, 041109 (2016).
- [22] R. Okugawa and S. Murakami, *Phys. Rev. B* **89**, 235315 (2014).
- [23] The valence bands cannot generally be trivialised over both blue and purple EBZs *simultaneously* due to the enclosed Weyl point. TRIM signs calculated for the blue T-plane cannot also be applied to the purple one, and different POS may be obtained in each case.
- [24] G. De Nittis and K. Gomi, *arXiv:1603.09421*.
- [25] See Supplemental Material for an overview of (co)homology, definitions and calculations of  $\mathcal{H}^n$ ,  $\mathcal{H}_n$ , Poincaré duality, bulk-boundary correspondence, and numerical methods.
- [26] Strictly speaking, closed paths are classified by the first *homotopy group*, but if we allow reordering of concatenated paths (*abelianization*), we recover  $H_1(X)$ . Physically, the loops correspond to the Fermi *locus* and the ordering does not matter.
- [27] Arcs connecting Weyl points can be thought of as loops upon identifying points in  $W$ .
- [28] R. Bott and L. Tu, *Differential Forms in Algebraic Topology*, Graduate Texts in Mathematics (Springer New York, 1995).
- [29] A. Hatcher, *Algebraic Topology*, Algebraic Topology (Cambridge University Press, 2002).
- [30] P. W. Gross and P. R. Kotiuga, *Electromagnetic Theory and Computation: A Topological Approach*, Math. Sci. Res. Inst. Pub. No. 48 (Cambridge Univ. Press, 2004).
- [31] K. Gomi and G. Thiang, (unpublished).
- [32] X.-L. Qi, T. L. Hughes, and S.-C. Zhang, *Phys. Rev. B* **78**, 195424 (2008).
- [33] D. J. Thouless, *Phys. Rev. B* **27**, 6083 (1983).
- [34] K. W. Kim, W.-R. Lee, Y. B. Kim, and K. Park, *Nat. Commun.* **7**, 13489 (2016).
- [35] Y. Hatsugai, *Phys. Rev. Lett.* **71**, 3697 (1993).
- [36] G. M. Graf and M. Porta, *Commun. Math. Phys.* **324**, 851 (2013).
- [37] J. C. Avila, H. Schulz-Baldes, and C. Villegas-Blas, *Math. Phys. Anal. Geom.* **16**, 137 (2013).
- [38] J. Kellendonk, T. Richter, and H. Schulz-Baldes, *Rev. Math. Phys.* **14**, 87 (2002).
- [39] D. Hsieh, Y. Xia, D. Qian, L. Wray, J. H. Dil, F. Meier, J. Osterwalder, L. Patthey, J. G. Checkelsky, N. P. Ong, A. V. Fedorov, H. Lin, A. Bansil, D. Grauer, Y. S. Hor, R. J. Cava, and M. Z. Hasan, *Nature* **460**, 1101 (2009).
- [40] V. Dwivedi and S. T. Ramamurthy, *Phys. Rev. B* **94**, 245143 (2016).
- [41] M. P. L. Sancho, J. M. L. Sancho, and J. Rubio, *Journal of Physics F: Metal Physics* **15**, 851 (1985).

# Supplemental Materials: Fu–Kane–Mele monopoles in semimetals

## S1. MATHEMATICAL ADDENDUM

### Homology, Fermi surfaces, and arcs

The  $n$ -th homology group  $H_n(X)$  of a space  $X$  is a topological invariant which detects “ $n$ -dimensional holes” in  $X$  [S1, S2]. For example,  $\mathbb{T}^2$  has two “1-dimensional holes” since the loops wrapping  $k_i, i = x, y$  cannot be contracted to a point within the BZ. This topological property is encoded by an abelian group  $H_1(\mathbb{T}^2) \cong \mathbb{Z}^2$ , and is relevant e.g. for classifying Fermi surfaces in 2D, which are closed 1-submanifolds that may wrap around such “holes”. Strictly speaking, non-contractible loops in  $X$  are classified by the first *homotopy group*  $\pi_1(X)$ , which is not generally abelian, but if we forget the ordering of loops (abelianisation), we do recover  $H_1(X)$ .

$H_1(X)$  is more precisely defined by considering continuous maps  $l$  from a 1-simplex  $[0, 1]$  into  $X$  (i.e. arcs that “sample” the topology of  $X$ ). The *boundary*  $\partial l$  of  $l$  is the formal difference  $l(1) - l(0)$ . A *1-chain* is a formal sum  $L = \sum_i m_i \cdot l_i, m_i \in \mathbb{Z}$ , and is called a *1-cycle* if its boundary  $\partial L \equiv \sum_i m_i \cdot \partial l_i$  vanishes (e.g. if  $L$  is actually a single map from a *circle* into  $X$ ).  $H_1(X)$  is then the 1-cycles modulo those which are obtainable from (some formal sum of) maps  $s_j : 2\text{-simplex} \rightarrow X$  by restriction to the boundary 1-simplices of  $s_j$  (such 1-cycles are called *1-boundaries*). In  $H_1(X)$ , the inverse of  $l$  can be represented by the same map but going around the circle in the opposite sense, denoted  $l^{\text{op}}$ . The higher-degree groups  $H_n(X)$  are defined in an analogous way using maps from  $n$ -simplices into  $X$  ( *$n$ -chains*). If the coefficients  $m_i$  come from some other abelian group  $G$ , we get the *homology groups with  $G$ -coefficients*  $H_n(X; G)$ . By default,  $H_n(X) \equiv H_n(X; \mathbb{Z})$ .

### Cohomology, Berry curvature, and valence bands

Cohomology groups with  $G$ -coefficients, denoted  $H^n(X; G)$ , are generally defined dually to homology, i.e. using homomorphisms from  $n$ -chains into  $G$  (called  *$n$ -cochains*), and there are *coboundary* maps  $d$ , *cocycles* etc. These groups are important for studying topological insulators/semimetals because they classify various types of vector bundles (or valence bands with various symmetries). For example, bundles of one-dimensional complex (resp. real) vector spaces over  $X$  are classified by  $H^2(X; \mathbb{Z})$ , (resp.  $H^1(X, \mathbb{Z}_2)$ ), and non-trivial 2D Chern insulators are possible due to  $H^2(\mathbb{T}^2; \mathbb{Z}) \cong \mathbb{Z}$ . For smooth manifolds  $X$ , the *de Rham cohomology groups*  $H_{\text{deRham}}^n(X; \mathbb{R})$  provide a more familiar model for the case  $G = \mathbb{R}$ ; they are given by the closed differential  $n$ -forms ( $d\omega = 0$ ) modulo the exact ones ( $\omega = d\eta$  for some  $\eta$ ). The inclusion of coefficients  $\mathbb{Z} \rightarrow \mathbb{R}$  induces a map  $H^n(X; \mathbb{Z}) \rightarrow H^n(X; \mathbb{R})$  so that we may study some (but not all) aspects of  $H^n(X; \mathbb{Z})$  using differential forms that integrate to integers on closed submanifolds. A typical example is the representation of the Chern class (a priori an element of  $H^2(X, \mathbb{Z})$ ) of a valence band by its Berry curvature 2-form  $\mathcal{F}$  (which gives an element of  $H^2(X, \mathbb{R})$ ).

### (Co)homology with T-symmetry

Fermionic T-symmetry ( $\mathbb{T}^2 = -1$ ) furnishes valence bands with a “Quaternionic” structure with respect to the momentum-reversing map  $\tau$ , i.e. it relates  $|\psi(k)\rangle$  to  $|\psi(\tau(k))\rangle$  antiunitarily (Kramers pair), and squares to  $-1$ . To classify such “Quaternionic” vector bundles, we need to use modified cohomology groups  $\mathcal{H}^2(X)$  [S3, S4], referred to in the main text, which are defined for every space  $X$  with  $\mathbb{Z}_2$ -action  $\tau$  and fixed point set  $F$ . An example is  $X$  a Brillouin torus,  $\tau : k \mapsto -k$ , and  $F$  the TRIM set. More precisely,  $\mathcal{H}^n(X) \equiv H_{\mathbb{Z}_2}^n(X, F; \tilde{\mathbb{Z}})$ , which is a  $\mathbb{Z}_2$ -equivariant cohomology group *relative to  $F$*  with *local coefficients*  $\tilde{\mathbb{Z}}$ . The meaning of  $\tilde{\mathbb{Z}}$  is that  $\mathbb{Z}_2$  also acts on the coefficients  $\mathbb{Z}$  by  $m \mapsto -m$ , and “equivariant” means that cochains are required to satisfy a certain  $\mathbb{Z}_2$ -symmetry condition with respect to  $\tau$ . These modifications keep track of the Kramers pair condition. Up to some mild technical assumptions,  $\mathcal{H}^2(X)$  classifies all possible T-invariant valence bands over  $X$  if  $\dim(X) \leq 3$  (with given even number of bands) [S3, S4].

The modified homology group  $\mathcal{H}_n(X)$ , referred to in the main text, is significantly simpler — it is the *equivariant* homology group  $H_n^{\mathbb{Z}_2}(X; \mathbb{Z})$  with ordinary integer coefficients. Intuitively, instead of probing  $X$  by mapping loops, surfaces, simplices etc. into  $X$  as in ordinary homology, we need to start with spaces  $Z$  that themselves have a  $\mathbb{Z}_2$  action, and “probe equivariantly”. For example, the 1-chains in  $\mathcal{H}_1(X)$  are, roughly speaking, maps  $l$  from 1D spaces  $Z$  with free involution  $\tau_{\text{free}}$  (i.e. having no fixed points) into  $X$  which satisfy  $\tau(l(z)) = l(\tau_{\text{free}}(z))$ . Thus each pair

of points  $z, \tau_{\text{free}}(z)$  is mapped onto a conjugate pair  $x, \tau(x)$  (which may coincide), and  $l$  traces out a T-stable 1D subspace of  $X$ . For T-stable subspaces  $Y \subset X$  (e.g. the Weyl point set  $W$ ), the *relative* homology group  $\mathcal{H}_1(X, Y)$  allows for T-stable *open* arcs that start and end in  $Y$ . In this way,  $\mathcal{H}_1(X, W)$  is relevant for classifying T-stable Fermi arcs.

If  $X$  has no  $\tau$ -fixed points (which is atypical), the equivariant homology  $H_n^{\mathbb{Z}_2}(X) \equiv \mathcal{H}_n(X)$  reduces to the *ordinary* homology of the naïve quotient space  $\check{X}$  obtained from  $X$  by identifying  $x \sim \tau(x)$ . Then, for instance, arcs  $\check{l}$  in  $\check{X}$  correspond to “doubled arcs”  $\check{l} \cup \tau(\check{l})$  in  $X$  which are exchanged by  $\tau$ , and conversely. However, it is harder to “properly divide” a  $\tau$ -stable arc that encounters fixed points. It is then necessary to use an auxiliary construction, called the *homotopy quotient* (or *Borel construction*), in place of  $\check{X}$ .

In Fig. S1, the quotient space  $\check{\mathbb{T}}^3$  for the BZ is illustrated, where further  $k \sim -k$  identifications are needed at the  $k_x = -\pi, 0$  faces. We also exhibit a loop in  $\check{\mathbb{T}}^3$  with the property that looping twice is contractible.

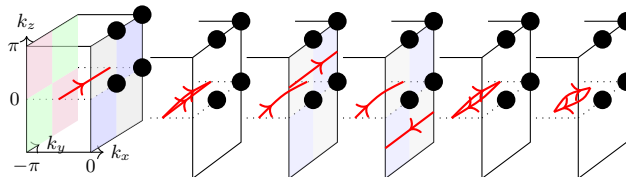


FIG. S1. (Left) The red loop  $\check{l}_y$  in  $\check{\mathbb{T}}^3$  is “half” of  $l_y$  (the dual arcs to  $\nu_y$ ). Starting from  $2\check{l}_y$ , deform one  $\check{l}_y$  into a loop on the  $k_x = 0$  face, identify it with its  $\tau$ -image, then deform it back to  $\check{l}_y^{\text{op}}$ . Thus  $2\check{l}_y \sim \check{l}_y + \check{l}_y^{\text{op}}$  which is contractible in  $\check{\mathbb{T}}^3$ .

### Topological bulk-boundary correspondence

In the presence of a boundary, only the momenta  $k_{\parallel}$  parallel to the boundary remain well-defined. A bulk Hamiltonian  $H$  with a spectral gap at the Fermi level  $E_F$  has a spectral projection  $p_F$  to the occupied states which defines the bulk invariant; partial Fourier-transform gives  $H(k_{\parallel})$  and a family of projections  $p_F(k_{\parallel})$ . With boundary conditions imposed,  $H(k_{\parallel})$  becomes a half-space operator  $\tilde{H}(k_{\parallel})$ , whose corresponding  $\tilde{p}_F(k_{\parallel})$  need not remain a projection. Intuitively, this means that new boundary-localised spectra with some  $k_{\parallel}$  is acquired at  $E_F$ . Since  $E_F$  may be varied within the bulk gap, one sees that the boundary spectra actually fills up this gap and connects a bulk valence band to a conduction band. In 2D,  $\tilde{H}(k_{\parallel})$  is just a periodic family over the edge momentum  $k_{\parallel}$ , and we can ask how many times the edge spectra “flows” past the Fermi level from below as the  $k_{\parallel}$ -circle is traversed around once (Fig. S2), c.f. the Thouless charge pump. Such edge indices (Bott–Maslov/Toeplitz indices), spectral flow [S5], and the connection to the bulk topological invariants were studied for the 2D case in [S6, S7], and for the quantum Hall effect in [S8] using a generalised cohomology theory called  $K$ -theory.

The (Toeplitz) bulk-boundary map of [S8] is formulated as a certain homomorphism  $\delta$  between bulk and boundary topological invariants. Abstractly,  $\delta$  is a kind of *push-forward/Gysin map* associated to the projection  $k \mapsto k_{\parallel}$ , which in the broken-T case is just integration along the transverse momenta  $k_{\perp}$  [S2]. Concretely,  $\delta(p_F)$  measures topologically the failure of  $\tilde{p}_F$  to remain a projection, and can be interpreted as counting *spectral flow*. In the T-symmetric case, the bulk-boundary map can be analogously defined to be “T-invariant integration”  $\mathcal{P}$ , as in the main text. The precise interpretation of  $\mathcal{P}$  as spectral flow in this case, especially in higher dimensions for semimetals, is not so well-understood and is the subject of ongoing investigation [S9]. Heuristically, the bulk band topology determines topological features of the boundary spectra. The latter is probed by the boundary Fermi surface which stays in the same topological class as the Fermi energy is varied within the bulk gap. Since the bulk band topology is classified cohomologically (e.g. through  $\mathcal{H}^2$ ), it is reasonable to expect the same for the boundary Fermi surface, at least in a dual sense (homologically, e.g. by  $\mathcal{H}_1$ ).

## S2. POINCARÉ DUALITY, INTEGRATION, AND INTERSECTION NUMBERS

If  $X$  is a closed oriented  $d$ -dimensional manifold, there is an isomorphism  $H^n(X) \cong H_{d-n}(X)$  for each  $n$ , known as Poincaré duality (PD) [S1, S2]. We are mainly concerned with  $d = 3$ , so  $H^2(X)$  is, under PD, the same thing as homology classes of arcs,  $H_1(X)$ . If  $M \subset X$  is a closed oriented 1-dimensional submanifold representing a class in  $H_1(X)$ , its PD in  $H^2(X)$  is a 2-form  $\omega$  satisfying  $\int_X \omega \wedge \eta = \int_M \eta$  for *all closed* 1-forms  $\eta$ . Intuitively, such an  $\omega$  “sees” all the directions normal to  $M$ . Another geometrical interpretation is that the PD of a  $(d - n)$ -cycle in an

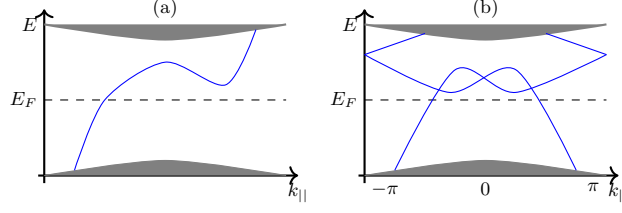


FIG. S2. (a) Family of edge states (blue) connecting bulk bands (gray) in broken-T case. The number of intersections (chiral edge states) at the Fermi level  $E_F$ , counted with signs, stays invariant as  $E_F$  is varied in the bulk gap. (b) Edge states in T-symmetric case. Although the signed intersection number at  $E_F$  always vanishes, the number of pairs of intersections (edge Kramers pairs) mod 2 is a  $\mathbb{Z}_2$ -invariant.

$d$ -manifold  $X$  is the  $n$ -cocycle that assigns to each  $n$ -cycle the number of (signed) intersections it has with the given  $(d-n)$ -cycle [S1].

To illustrate the basic idea of PD in the context of topological insulators, consider a weak 3D Chern insulator built from layers of unit-Chern-number 2D insulators parallel to the  $y$ - $z$  directions. Its Berry curvature  $\mathcal{F}$  is such that the integral over  $k_y$ - $k_z$  is the non-zero weak Chern number  $c_1^{yz} = 1$ , while the integrals over  $k_x$ - $k_y$  and  $k_x$ - $k_z$  vanish, thus  $\mathcal{F}$  is  $dk_y \wedge dk_z$  up to some exact form and  $2\pi$  factors.  $\mathcal{F}$  is PD to (any) circle  $S_x^1$  wrapping  $k_x$  once, since it is easy to verify that  $\int_{\mathbb{T}^3} \mathcal{F} \wedge \eta = \int_{S_x^1} \eta$  for all closed 1-forms  $\eta$ : we only need to check  $\eta = f(k)dk_x$ , and  $d\eta = 0$  ensures that  $\int_{S_x^1} \eta$  does not depend on the  $k_y, k_z$  coordinates of  $S_x^1$ . Thus this weak Chern insulator may be represented by the circle  $S_x^1$  (at any  $k_y, k_z$ ).

If we integrate  $\mathcal{F}$  over  $k_y$ , we are left with a 1-form  $dk_z$  on the surface BZ  $\mathbb{T}^2$ , whose PD (in  $\mathbb{T}^2$ ) is now  $S_x^1 \subset \mathbb{T}^2$  and turns out to be the surface Fermi circle. Thus  $\text{PD}(\int_{S_y^1} \mathcal{F}) = p(\text{PD}(\mathcal{F}))$  where  $p$  is the map projecting out  $k_y$ , i.e.  $p$  is Poincaré dual to integrating over  $k_y$ . Furthermore,  $S_x^1$  generically intersects (transversally in the BZ) the  $k_y$ - $k_z$  subtorus once but not the other subtori, and these intersection numbers recover the weak Chern numbers  $c_1^{yz} = 1, c_1^{xy} = 0 = c_1^{zx}$ .

With some assumptions on  $(X, \tau)$ , a variant of PD holds for  $\mathcal{H}^\bullet$  and  $\mathcal{H}_\bullet$  [S9]. For example, there are isomorphisms  $\mathcal{H}^n(\mathbb{T}^3) \cong \mathcal{H}_{3-n}(\mathbb{T}^3)$  and  $\mathcal{H}^n(\mathbb{T}^3 \setminus W) \cong \mathcal{H}_{3-n}(\mathbb{T}^3, W)$  for  $n \geq 2$  and  $W$  a finite set of points avoiding the TRIM.

### Global invariants for T-WSM and local charge cancellation

For 2D/3D TI, the T-stable valence bands can always be trivialised (global choice of Bloch eigenstates), and one can prove that  $\mathcal{H}^2(\mathbb{T}^d)$ ,  $d = 2, 3$  “localises” completely to data at the TRIM. Explicitly, this means that  $\mathcal{H}^2(\mathbb{T}^d)$  is given by sign maps  $F \rightarrow \{\pm\}$  modulo global T-gauge transformations over  $\mathbb{T}^d$ , recovering the POS formulae for the FKMI [S3]. However, for 3D T-WSM, it is not possible to make a global choice of valence Bloch eigenstates everywhere on  $\mathbb{T}^3 \setminus W$ , so signs cannot be assigned to all the TRIM at once. Nevertheless, we can still compute the group  $\mathcal{H}^2(\mathbb{T}^3 \setminus W) \cong \mathcal{H}_1(\mathbb{T}^3, W)$  of T-WSM invariants using a general “locality principle”. This is called the *Mayer-Vietoris* property of (co)homology [S2], which is a kind of inclusion-exclusion principle that allows topological invariants of  $X$  to be computed from (i) those of T-stable-subspaces  $\{X_i\}_{i \in I}$  that cover  $X$ , and (ii) those of their intersections.

Consider the simplest T-WSM with two pairs of Weyl points  $W = \{\pm w, \pm w'\}$  disjoint from the TRIM, as in the main text. Note that  $w$  and  $-w$  have the same Weyl charge by T-symmetry, as do  $w'$  and  $-w'$ . Take  $X_1 = \mathbb{T}^3 \setminus W$  and  $X_2 = D_W$  where  $D_W$  is the disjoint union of small open balls surrounding the Weyl points, then  $X_1 \cap X_2$  is (retractable to)  $S_W^2 \equiv S_w^2 \amalg S_{-w}^2 \amalg S_{w'}^2 \amalg S_{-w'}^2$ . The Mayer-Vietoris principle organises the  $\mathcal{H}^\bullet, \mathcal{H}_\bullet$  of all these spaces, by producing the sequence (c.f. [S10])

$$\begin{array}{ccccccc}
 0 & \longrightarrow & \overbrace{\mathcal{H}^2(\mathbb{T}^3)}^{\text{TI invariants}} & \xrightarrow{\text{restriction of bands}} & \overbrace{\mathcal{H}^2(\mathbb{T}^3 \setminus W)}^{\text{T-WSM invariants}} & \xrightarrow{\text{restriction of bands}} & \overbrace{\mathcal{H}^2(S_W^2)}^{\text{T-WSM local Weyl charges}} & \xrightarrow{\text{sum}} & \overbrace{\mathcal{H}^3(\mathbb{T}^3)}^{\text{total charge}} & \longrightarrow & 0 \\
 & & \downarrow \text{PD} & & \downarrow \text{PD} & & \downarrow \text{PD} & & \downarrow \text{PD} & & \\
 0 & \longrightarrow & \underbrace{\mathcal{H}_1(\mathbb{T}^3)}_{\text{Dual TI arcs}} & \longrightarrow & \underbrace{\mathcal{H}_1(\mathbb{T}^3, W)}_{\text{Dual T-WSM arcs}} & \xrightarrow{\partial} & \mathcal{H}_0(W) & \longrightarrow & \mathcal{H}_0(\mathbb{T}^3) & \longrightarrow & 0
 \end{array}$$



in which both the horizontal sequences are exact (i.e. the kernel of one map *equals* the image of the previous map) and the vertical maps are Poincaré duality isomorphisms. Note that  $D_W$  does not contribute because it is contractible to (the Weyl) points. The local Weyl charge group for T-WSM is  $\mathbb{Z}^2$ , given by the Weyl charges of  $w$  and  $w'$ .

Exactness is precisely the useful property for computation and physical interpretation. For example, exactness at  $\mathcal{H}^2(S_W^2)$  means that when a T-WSM is restricted to the spheres  $S_W^2$  surrounding the Weyl points (image of the second restriction map), the local charges must cancel (kernel of the sum map), and furthermore, every charge-cancelling configuration can arise in some T-WSM. This is the precise charge-cancellation condition for T-WSM, included here because the Nielsen–Ninomiya argument (used for ordinary WSM) does not work verbatim.

The top sequence is, explicitly,

$$0 \rightarrow \mathbb{Z}_2^4 \rightarrow \mathcal{H}^2(\mathbb{T}^3 \setminus W) \cong \mathcal{H}_1(\mathbb{T}^3, W) \rightarrow \mathbb{Z}^2 \xrightarrow{\text{sum}} \mathbb{Z} \rightarrow 0 \dots$$

from which we deduce that  $\mathcal{H}^2(\mathbb{T}^3 \setminus W) \cong \mathcal{H}_1(\mathbb{T}^3, W) \cong \mathbb{Z}_2^4 \oplus \mathbb{Z}$ . The  $\mathbb{Z}_2^4$  factors are the usual TI invariants  $\nu_0, \nu_i$ , while the new integer invariant  $q \in \mathbb{Z}$  counts the number of (reference) “open arcs” connecting  $\pm w'$  to  $\pm w$ . As in the main text, a pair of open arcs connecting  $\pm w'$  to  $\mp w$  represents  $(\nu_0; \nu_i; q) = (-; +, +, +; 1)$ , and generates a *different* copy of  $\mathbb{Z}$  in  $\mathcal{H}_1(\mathbb{T}^3, W)$ . Thus a particular choice of reference Weyl point connection just selects the  $\mathbb{Z}$  basis element for the T-WSM invariants (i.e. it specifies one of many possible factorisations of  $\mathcal{H}_1(\mathbb{T}^3, W)$  into  $\mathbb{Z}_2^4 \oplus \mathbb{Z}$ ). If there are  $q$  pairs of Weyl points,  $W = \{\pm w_i\}_{i=1, \dots, q}$ , we have  $\mathcal{H}_1(\mathbb{T}^3, W) \cong \mathbb{Z}_2^4 \oplus \mathbb{Z}^{q-1}$  where the factorisation again depends on a choice of reference connections (e.g. for each  $i = 1, \dots, q-1$ , we can choose a pair of connections from  $\pm w_i$  to  $\pm w_{i+1}$  to generate a  $\mathbb{Z}$ ).

### S3. SPECTRAL DENSITY FOR THE INTERFACE LAYER

In order to find localized modes between two distinct systems, we used the method based on Green’s function provided in Refs. S11 and S12. Suppose that the Hamiltonian is given by

$$\begin{aligned} H &= \sum_{n,m} \left( H_n \delta_{n,m} + V_n \delta_{n,m-1} + V_{n-1}^\dagger \delta_{n,m+1} \right) e_{n,m}, \\ &= \sum_n \left( H_n e_{n,n} + V_n e_{n,n+1} + V_n^\dagger e_{n+1,n} \right), \end{aligned}$$

where  $n, m$  label layers,  $H_n$  and  $V_n$  are  $M \times M$  matrixes with  $M$  being the number of internal degrees of freedom, and  $e_{n,m}$  are shift operators from position  $m$  to  $n$ . Let us consider the case in which system A is stacked on top of B. The corresponding Hamiltonian is described by  $H_n = h_A(h_B)$  for  $n < 0$  ( $n > 0$ ),  $H_0 = \tilde{h}$ , and  $V_n = v_A(v_B)$  for  $n \leq -1$  ( $n \geq 0$ ). The Green’s function is then defined by  $(\omega I - H)G(\omega) = I$ , where  $I$  is the identity matrix corresponding to the dimension of  $H$ . Letting  $G_{n,m}$  be  $M \times M$  block part of the Green’s function, which pertains to  $n$ -th and  $m$ -th layers, we find the following set of equations:

$$\begin{aligned} (\omega I_M - \tilde{h}) G_{0,0} &= I_M + v_A^\dagger G_{-1,0} + v_B G_{1,0}, \\ (\omega I_M - h_A) G_{n,0} &= v_A^\dagger G_{n-1,0} + v_A G_{n+1,0}, \quad \text{for } n \leq -1, \\ (\omega I_M - h_B) G_{n,0} &= v_B^\dagger G_{n-1,0} + v_B G_{n+1,0}, \quad \text{for } n \geq 1, \end{aligned}$$

with  $I_M$  being  $M \times M$  identity matrix. The spectral density of the localized mode at the interface is related to  $G_{0,0}$ , which can be found by recursively solving the above set of equations. Defining the following relations for the first step in the recursion

$$\begin{aligned} \alpha_1^{A,B} &= v_{A,B} (\omega I_M - h_{A,B})^{-1} v_{A,B}, \\ \beta_1^{A,B} &= v_{A,B}^\dagger (\omega I_M - h_{A,B})^{-1} v_{A,B}^\dagger, \\ \kappa_1^{A,B} &= v_{A,B} (\omega I_M - h_{A,B})^{-1} v_{A,B}^\dagger, \\ \lambda_1^{A,B} &= v_{A,B}^\dagger (\omega I_M - h_{A,B})^{-1} v_{A,B}, \\ h_0^{A,B} &= h_{A,B}, \quad h_0 = \tilde{h}, \end{aligned}$$

the set of relations in  $l$ -th step are given by

$$\begin{aligned} h_l^{A,B} &= h_{l-1}^{A,B} + \kappa_l^{A,B} + \lambda_l^{A,B}, & h_l &= h_{l-1} + \kappa_l^B + \lambda_l^A, \\ \alpha_l^{A,B} &= \alpha_{l-1}^{A,B} \left( \omega I_M - h_{l-1}^{A,B} \right)^{-1} \alpha_{l-1}^{A,B}, \\ \beta_l^{A,B} &= \beta_{l-1}^{A,B} \left( \omega I_M - h_{l-1}^{A,B} \right)^{-1} \beta_{l-1}^{A,B}, \\ \kappa_l^{A,B} &= \alpha_{l-1}^{A,B} \left( \omega I_M - h_{l-1}^{A,B} \right)^{-1} \beta_{l-1}^{A,B}, \\ \lambda_l^{A,B} &= \beta_{l-1}^{A,B} \left( \omega I_M - h_{l-1}^{A,B} \right)^{-1} \alpha_{l-1}^{A,B}, \end{aligned}$$

and the set of the equations for the Green's function in  $l$ -th step are obtained as follows:

$$\begin{aligned} (\omega I_M - h_l) G_{0,0} &= I_M + \beta_l^A G_{-2^l,0} + \alpha_l^B G_{2^l,0}, \\ (\omega I_M - h_l^A) G_{n,0} &= \beta_l^A G_{n-2^l,0} + \alpha_l^A G_{n+2^l,0}, & \text{for } n \leq -2^l, \\ (\omega I_M - h_l^B) G_{n,0} &= \beta_l^B G_{n-2^l,0} + \alpha_l^B G_{n+2^l,0}, & \text{for } n \geq 2^l. \end{aligned}$$

Typically  $\alpha_l^{A,B}$  and  $\beta_l^{A,B}$  reduce in magnitude as  $l$  increases, so we can approximate the Green's function at zeroth layer by  $G_{0,0}(\omega) \approx (\omega I_M - h_l)^{-1}$ . The spectral function at the zeroth layer is then given by  $A_{0,0}(\omega) = -(2\pi)^{-1} \text{Im} \{ \text{Tr} [G_{0,0}(\omega + i\delta)] \}$ , where we let  $\omega \rightarrow \omega + i\delta$  with  $\delta$  being a sufficiently small real number.

For a concrete example giving Fig. 5(a)-(d) in the main text, we can choose the Hamiltonian for the system A to be

$$\begin{aligned} h_A(k_x, k_z) &= a \sin k_x \tau_1 \otimes \sigma_3 + \beta \tau_2 \otimes \sigma_2 + d \tau_2 \otimes \sigma_3 + [t \cos k_z + 2b(2 - \cos k_x)] \tau_3 \otimes \sigma_0 + \lambda \sin k_z \tau_0 \otimes \sigma_1 \\ v_A &= b \tau_3 \otimes \sigma_0 + \frac{i}{2} (a \tau_2 \otimes \sigma_0 + \alpha \tau_1 \otimes \sigma_2), \end{aligned}$$

which are obtained from the tight-binding model for a time-reversal invariant Weyl semimetal given in Ref. S12 by only Fourier transforming  $x$ - and  $z$ -directions. Here,  $\tau_0$  and  $\sigma_0$  are  $2 \times 2$  identity matrixes, and  $\tau_i$  and  $\sigma_i$  are Pauli matrixes. Furthermore, we set the system B by exchanging  $k_x$  and  $k_z$  and inverting the coordinate in  $y$ -direction from the system A, which translates to

$$\begin{aligned} h_B(k_x, k_z) &= h_A(k_z, k_x), \\ v_B &= b \tau_3 \otimes \sigma_0 - \frac{i}{2} (a \tau_2 \otimes \sigma_0 + \alpha \tau_1 \otimes \sigma_2). \end{aligned}$$

For the zeroth layer part of the Hamiltonian, we let  $\tilde{h} = (h_A + h_B)/2$ . We chose the parameters in the Hamiltonian to be  $a = 1$ ,  $b = 1$ ,  $t = 1.5$ ,  $d = 0.1$ ,  $\alpha = 0.3$ ,  $\lambda = 0.5$ , and  $\beta = 0.4$ . Figure 5(c) can then be found by evaluating  $A_{0,0}(\omega)$ , which corresponds to the spectral density of the localized state at zeroth layer. Figure. 5 (a) (Fig. 5(b)) corresponds to the spectral density of the surface states of the system A (B) by itself, which is obtained by turning off the contribution from the system B (A) by setting  $h_B(h_A) = 0$ ,  $v_B(v_A) = 0$  and  $\tilde{h} = h_A(h_B)$  in evaluating  $A_{0,0}(\omega)$ . For Fig. 5(d), we calculated the spectral densities of the surface state of the system A for various values of  $\omega$ .

- 
- [S1] A. Hatcher, *Algebraic Topology*, Algebraic Topology (Cambridge University Press, 2002).  
[S2] R. Bott and L. Tu, *Differential Forms in Algebraic Topology*, Graduate Texts in Mathematics (Springer New York, 1995).  
[S3] G. De Nittis and K. Gomi, *Commun. Math. Phys.* **339**, 1 (2015).  
[S4] G. De Nittis and K. Gomi, [arXiv:1603.09421](https://arxiv.org/abs/1603.09421).  
[S5] Y. Hatsugai, *Phys. Rev. Lett.* **71**, 3697 (1993).  
[S6] G. M. Graf and M. Porta, *Commun. Math. Phys.* **324**, 851 (2013).  
[S7] J. C. Avila, H. Schulz-Baldes, and C. Villegas-Blas, *Math. Phys. Anal. Geom.* **16**, 137 (2013).  
[S8] J. Kellendonk, T. Richter, and H. Schulz-Baldes, *Rev. Math. Phys.* **14**, 87 (2002).  
[S9] K. Gomi and G. Thiang, (unpublished).  
[S10] V. Mathai and G. C. Thiang, *J. Phys. A: Math. Theor. (Letter)* **50**, 11LT01 (2017).  
[S11] M. P. L. Sancho, J. M. L. Sancho, and J. Rubio, *Journal of Physics F: Metal Physics* **15**, 851 (1985).  
[S12] A. Lau, J. van den Brink, and C. Ortix, [arXiv:1701.01660](https://arxiv.org/abs/1701.01660).